DOI: 10.1002/ange.201300711

Metal-Free Electrocatalysts

Molecular Architecture of Cobalt Porphyrin Multilayers on Reduced Graphene Oxide Sheets for High-Performance Oxygen Reduction Reaction**

Hongjie Tang, Huajie Yin, Jiangyan Wang, Nailiang Yang, Dan Wang, and Zhiyong Tang**

Thanks to their lightweight, highly efficient, modular and scalable properties, polymer electrolyte membrane fuel cells (PEMFCs) have long been thought to be a promising candidate for applications in transportation and in both stationary and portable electronics.[1] Unfortunately, despite the above advantages, until now the fuel-cell technologies have failed to reach mass commercialization, and the main problems include short operational time and high cost of the materials used.[1b–d] For example, platinum-based materials are generally believed to be ideal catalysts for the oxygen reduction reaction (ORR) at the cathodes of PEMFCs; however, their disadvantages, for example, low tolerance to methanol fuel, high price and scarcity, limit the practical application of platinum-based catalysts.[2] Therefore, replacement of platinum-based materials with non-precious-metal catalysts, which are of low cost, high catalytic activity, and robust, has become one of the key issues for the realization of mass applications of PEMFCs.[3a,b]

In recent years, many non-precious-metal electrocatalysts have been investigated, such as non-pyrolyzed transition-metal macrocycles, conductive polymer based complexes, transition-metal chalcogenides,[3c,d] metal oxide/carbide/nitride materials, and even enzymes.[3a] One of the most promising types of non-precious-metal catalysts is carbon-supported transition-metal-nitrogen (C/M-N_x) materials (M = Co, Fe, Ni, Mn, etc., and normally $x = 2$ or 4).[4] The purpose of using carbon substrates to support M-N_x is that they have high surface areas and can offer a sufficient number of reacting sites.[5] Since the finding in the 1960s that the carbon-supported transition-metal porphyrins, namely cobalt phthalocyanine (CoPc), could act as the catalysts for ORR,[6] many C/M-N_x compounds have been investigated and their potential applications in PEMFCs have been demonstrated.[7] However, all these C/M-N_x catalysts still suffer from low activity and stability toward ORR and are thus far away from satisfying the requirements of fuel cells.[8] The drawbacks of the C/M-N_x catalysts originate from the absence of control of the interaction between the C substrates and the M-N_x compounds as well as the rational structural design of the M-N_x compounds.[3a]

Herein, we present a novel strategy to prepare the C/M-N_x catalysts, in which the molecular architecture of the cobalt porphyrin multilayers is incorporated onto the reduced graphene oxide (rGO) sheets using the layer-by-layer (LBL) assembly technique.[9] In addition to its high specific surface area,[10] rGO can offer possible electrostatic or coordination interactions with the supported catalysts.[11] Especially for the cobalt porphyrin catalysts, the planar benzene rings of the rGO sheets could provide additional interactions, for example, π–π stacking and van del Waals forces. Such multiple interactions will favor the stability of the catalysts on the substrates.[12] Also the rGO sheets have high chemical, thermal, and mechanical stabilities, which are beneficial for improvement of the lifetime of the catalysts.[13] On the other hand, the LBL assembly method has been broadly used to construct functional nanostructures because of its numerous advantages, such as ease of preparation, versatility, capability of incorporating high loadings of different molecules in the films.[14a] Therefore, we expect to use the LBL assembly technique to control the structure, thickness, and uniformity of the cobalt porphyrin catalysts on the surface of the rGO sheets at the molecular level, leading to maximization of the catalytic activity for ORR.

Scheme 1 illustrates the typical LBL procedure to synthesize the catalysts. First, the graphene oxide (GO) and Co^{2+} ions are mixed in the solution. The presence of many oxygen-containing groups on the surface of the GO sheets allows the Co^{2+} ions in the solution to be adsorbed onto the GO sheets by coordination/electrostatic interactions.[11b] Subsequently, the GO sheets with adsorbed Co^{2+} ions are separated from the mixture solution by centrifugation and washed with pure water several times, to remove excess Co^{2+} ions. Then, the Co^{2+}–GO sheets are mixed with 5,10,15,20-tetrakis(4-hydroxyphenyl) porphyrin (THPP) in solution.[9b] Afterwards, the GO sheets with the adsorbed Co^{2+}–THPP monolayer are purified again by centrifugation and washing with pure water. As a result, the desired multilayers on the GO substrate can

[*] H. Tang, J. Wang, N. Yang, Prof. D. Wang
State Key Laboratory of Multiphase Complex Systems, Institute of Process Engineering, Chinese Academy of Sciences
Beijing 100190 (P.R. China)
E-mail: danwang@mail.ipe.ac.cn
H. Tang, H. Yin, Prof. Z. Tang
National Center for Nanoscience and Technology
No.11, Beiyitiao, Zhongguancun, Beijing 100190 (P. R. China)
E-mail: zytang@nanoctr.cn
H. Tang, J. Wang, N. Yang
University of Chinese Academy of Sciences
No. 19A Yuquan Road, Beijing 100049 (P. R. China)

[**] This work was partially supported by the National Natural Science Foundation for Distinguished Youth Scholars of China (21025310, Z.Y.T.), National Natural Science Foundation of China (91027011, Z.Y.T.; 21031005, D.W.; 91122014, D.W.), and National Research Fund for Fundamental Key Project (2009CB930401, Z.Y.T.)

Supporting information for this article is available on the WWW under http://dx.doi.org/10.1002/anie.201300711.

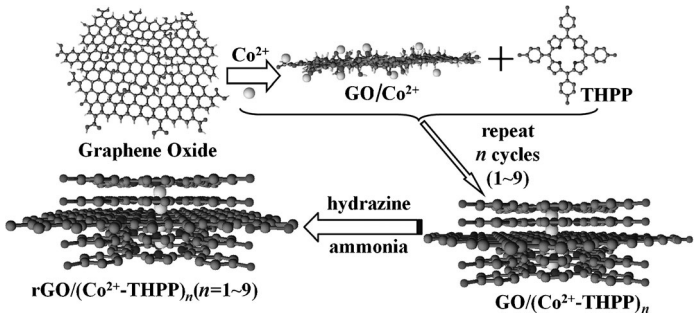

Scheme 1. Preparation procedure of rGO/$(Co^{2+}$–THPP$)_n$.

be obtain the by many cycles of alternative adsorption of Co^{2+} and THPP. Such nanostructures are named as GO/$(Co^{2+}$–THPP$)_n$, and *n* stands for the cycle number of one composite layer of Co^{2+} and THPP.[9c,14b] Finally, the GO supports in the GO/$(Co^{2+}$–THPP$)_n$ composites are reduced by hydrazine in the ammonia solution to obtain the rGO/$(Co^{2+}$–THPP$)_n$ products.[11b]

The LBL assembly process of the Co^{2+}–THPP multilayers on the GO sheets is monitored by the UV/Vis absorption spectra (Figure 1).[14c] The free THPP molecules in solution display five characteristic absorption bands (Figure 1 a), including an intense Soret band at 413 nm and four Q-bands located at 516, 554, 594, and 650 nm. Coordination of THPP with Co^{2+} ions to form the Co^{2+}–THPP complexes results in red shift of the Soret bands to 433 nm, while the number of Q-bands decreases to two (inset in Figure 1 a).[15a] Compared to that of free THPP or Co^{2+}–THPP molecules in solution, the Soret band of the Co^{2+}–THPP mutilayers on the GO sheets is split into two peaks, 425 nm and 452 nm (Figure 1 b), which should be assigned to the J-aggregation in the same plane and the H-aggregation along the axial direction, respectively.[15b] Furthermore, by normalizing the adsorption peak of the GO sheets at 229 nm, it can be seen that the intensity of the Soret bands of GO/$(Co^{2+}$–THPP$)_n$ at 425 nm increases linearly with the assembly cycle, suggesting the uniform growth of the Co^{2+}–THPP multilayers perpendicular to the GO substrates.[16]

Such homogeneous growth can be also confirmed by atomic force microscopy (AFM; Supporting Information, Figure S1). The measured thickness of the single GO layer before deposition of the Co^{2+}–THPP complexes is around 1.3 nm (Figure S1a),[17a] and the average thickness of each layer during the subsequent growth is measured to be about 0.5 nm (Figure S1 and S2). Notably, half of this value (Co^{2+}–THPP should be absorbed on both sides of the GO sheets) is very close to the thickness of the Co^{2+}–THPP molecule (0.3 nm),[17b] which suggests that, in each layer, Co^{2+}–THPP is homogenously adsorbed on the GO sheets in the form of monolayer.

To enhance the conductivity in the ORR process, the GO/$(Co^{2+}$–THPP$)_n$ samples are subsequently reduced by hydrazine in ammonia solution.[11b] As shown in Figure 1 c, the resultant rGO/$(Co^{2+}$–THPP$)_7$ products in solution are very stable and no precipitation is observed even after being left for five months at room temperature. This stability is essential for lowering the overpotential of the ORR catalysts;[18] whereas the direct reduction of the GO sheets in solution results in considerable precipitation after the same time. Figure 1 d shows the UV/Vis absorption spectra of GO/$(Co^{2+}$–THPP$)_7$, rGO/$(Co^{2+}$–THPP$)_7$, GO and rGO. Both GO and GO/$(Co^{2+}$–THPP$)_7$ show the characteristic absorption peaks of GO at 229 nm (Figure 1 d). After reduction, for both the rGO and rGO/$(Co^{2+}$–THPP$)_7$ products, the peaks at 229 nm are red shifted to 266 nm with a clear increase of the adsorption intensity in the whole UV and visible region.[11,12] Another prominent absorption feature of the rGO/$(Co^{2+}$–THPP$)_7$ products is that the characteristic Soret band of Co^{2+}–THPP is preserved with slight bathochromic shift to 433 nm, indicating that reduction with hydrazine only results in conversion of GO to rGO rather than any reaction with the Co^{2+}–THPP multilayers. The red shift of the Soret band absorption can be assigned to the increased electron transfer from the rGO substrates to the THPP molecules through the Co^{2+} bridge. Such electron transfer gives rise to the electron-rich Co^{2+}–THPP complexes, which is beneficial for ORR.[19] This conclusion is also drawn by microscopy observation (Figure S3a and S3b), and there is no structural alteration to be found after reduction (Figure S4).

Except for the morphology, possible changes in the chemical composition of rGO/$(Co^{2+}$–THPP$)_7$ by hydrazine reduction are investigated by X-ray photoelectron spectroscopy (XPS). Figure 2 displays the high-resolution

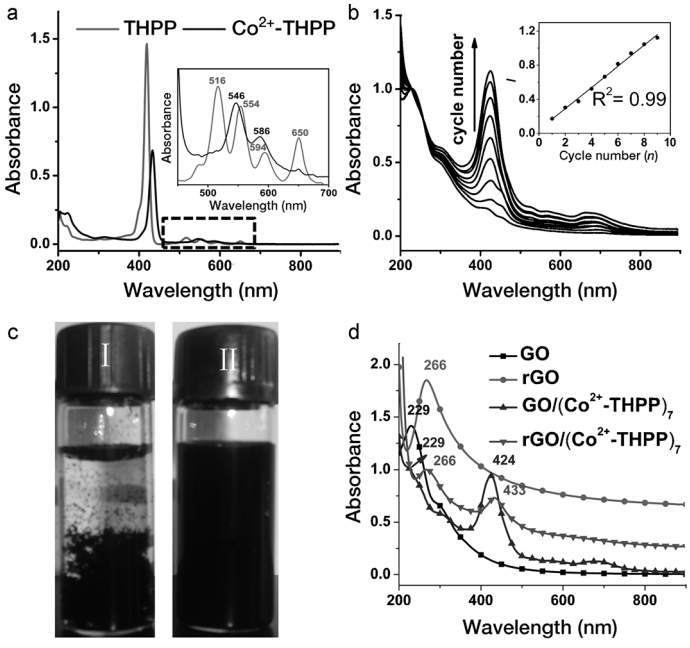

Figure 1. a) UV/Vis adsorption spectra of free THPP or Co^{2+}–THPP in solution. Inset: expansion of the selected area. b) UV/Vis adsorption spectra of GO/$(Co^{2+}$–THPP$)_n$ ($n = 1$–9). Inset: relationship of the UV/Vis adsorption intensity at 425 nm with increase of the cycle number. c) Solutions of rGO (I) and rGO/$(Co^{2+}$–THPP$)_7$ (II) after being stored under ambient conditions for five months. d) UV/Vis adsorption spectra of GO, rGO, GO/$(Co^{2+}$–THPP$)_7$, and rGO/$(Co^{2+}$–THPP$)_7$.

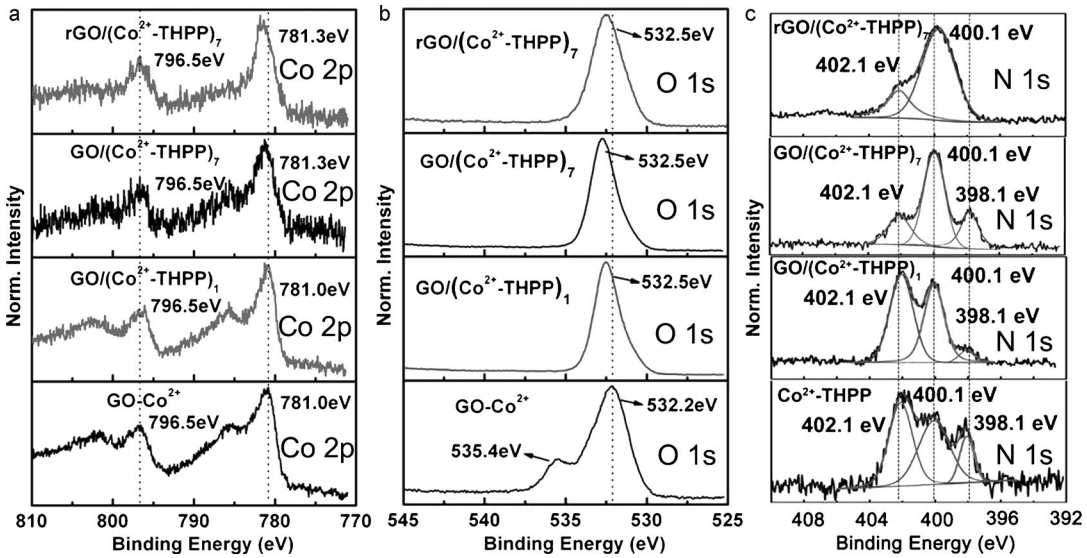

Figure 2. High-resolution XPS spectra of a) Co 2p and b) O 1s of GO/Co^{2+}, GO/(Co^{2+}–THPP)$_1$, GO/(Co^{2+}-THPP)$_7$, and rGO/(Co^{2+}–THPP)$_7$, and c) N 1s of Co^{2+}–THPP, GO/(Co^{2+}–THPP)$_1$, GO/(Co^{2+}–THPP)$_7$, and rGO/(Co^{2+}–THPP)$_7$.

spectra of Co 2p and O 1s of GO/Co^{2+}, GO/(Co^{2+}–THPP)$_1$, GO/(Co^{2+}–THPP)$_7$, and rGO/(Co^{2+}–THPP)$_7$ and the N 1s of Co^{2+}–THPP, GO/(Co^{2+}–THPP)$_1$, GO/(Co^{2+}–THPP)$_7$, and rGO/(Co^{2+}–THPP)$_7$. As shown in Figure 2a, direct mixture of the GO sheets with the Co^{2+} ions leads to appearance of the Co 2p peaks located at 781.0 eV and 796.5 eV. Simultaneously, in addition to the O 1s peak of GO at 532.2 eV (Figure S5b), a new O 1s peak located at 535.4 eV arises (GO/Co^{2+} in Figure 2b), which corresponds to the electrostatic interaction of the Co^{2+} ions and the oxygen-containing groups of the GO substrates.[20] After injection of the THPP molecules, the O 1s peak at 535.4 eV disappears and the peak located at 532.2 eV shifts to 532.5 eV (GO/(Co^{2+}–THPP) in Figure 2b), whereas the Co 2p peaks remain unchanged. Therefore, one can draw the conclusion that after introduction of the N-containing THPP molecules, the Co^{2+}–THPP complexes are formed while the interactions between the Co^{2+} ions and the O-containing groups of the GO substrates are weakened. This deduction is also supported by analyzing the XPS spectra of the N species. As for the Co^{2+}–THPP complexes in solution, a new peak with respect to pure THPP (Figure S5c)[21a] appears at 402.1 eV, which is assigned to the N atoms binding Co^{2+} ions (Figure 2c). The coexistence of the three types of N 1s signals indicates that the N atoms of the THPP macrocycles only partially coordinate with the Co^{2+} ions to form the complexes. Similarly to the Co^{2+}–THPP complexes, the three types of N 1s signals are distinguished in GO/(Co^{2+}–THPP)$_1$, though the intensity of the iminic N at 398.1 eV is decreased through more coordination with Co^{2+} ions. When the cycle number is increased to 7, the intensity of the Co^{2+}–N peak at 402.1 eV in GO/(Co^{2+}–THPP)$_7$ is considerably decreased, revealing that many THPP molecules in the Co^{2+}–THPP multilayers may not coordinate with the Co^{2+} ions. The strong intermolecular π–π interactions between the adjacent THPP layers should be responsible for stabilization of such uncoordinated THPP molecules in the multilayer structure. After production of rGO/(Co^{2+}–THPP)$_7$ by reduction with hydrazine, the signal corresponding to the iminic N atom at 398.1 eV has almost disappeared, indicating that the iminic N atom of the THPP molecules is reduced to a pyrrolic N atom.[21b] Nevertheless, the signal of Co^{2+}–N at 402.1 eV is well-preserved in rGO/(Co^{2+}–THPP)$_7$, highlighting the high stability of rGO/(Co–THPP)$_n$ even in the strong reductive environment. This high-stability feature will aid use of the composites as durable ORR catalysts.

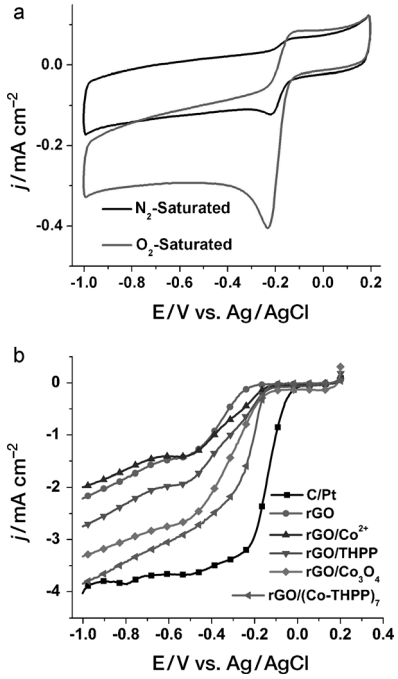

Figure 3. a) CV curves of rGO/(Co^{2+}-THPP)$_7$ on glass carbon electrodes in O_2-saturated or N_2-saturated 0.1 M KOH solution. b) LSV on RDE of rGO, rGO/Co^{2+}, rGO/THPP, rGO/Co_3O_4, rGO/(Co^{2+}–THPP)$_7$, and C/Pt in O_2-saturated 0.1 M KOH solution with a sweep rate of 10 mV s^{-1}. The rotation rate of RDE is 1600 rpm.

The electrocatalytic activity of rGO/$(Co^{2+}$–THPP$)_n$ for ORR is evaluated by cyclic voltammetry (CV) scanning in a 0.1 M KOH aqueous solution saturated with either N_2 or O_2 gas at room temperature.[22] The rGO/$(Co^{2+}$–THPP$)_7$ sample is selected as a typical catalyst for examining the ORR activity. As shown in Figure 3a, a well-defined O_2 reduction peak centered at −0.22 V emerges as the electrolyte solution is saturated with O_2 (the gray curve in Figure 3a), which is close to the value of −0.18 V of the commercial carbon-supported Pt (C/Pt) and superior to other rGO-based catalysts (Figure S6 and S7). The impressive electrocatalytic activity of rGO/$(Co^{2+}$–THPP$)_7$ is confirmed by recording the linear sweep voltammetry (LSV) curves on a rotating disk electrode (RDE; Figure 3b). The limiting current density of rGO/$(Co^{2+}$–THPP$)_7$ at −1.0 V is up to about −4.0 mA cm^{-2}, which is much higher than other rGO-based materials and comparable to C/Pt. The electrocatalytic activity of rGO/$(Co^{2+}$–THPP$)_7$ should originate from the synergistic effect of the adsorbed Co^{2+}–THPP complexes and the rGO substrates in the hybrid materials.

The LBL assembly technique allows us to accurately control the structure and the thickness of the Co^{2+}–THPP complexes on the rGO substrates.[14] As shown in Figure S8, with the increasing layer number of the Co^{2+}–THPP complexes, the peak position of ORR is positively shifted until the layer number reaches 5. The rGO/$(Co^{2+}$–THPP$)_n$ composites with $n > 5$ have similar ORR peaks at around −0.18 V. Such a change in the ORR activity could be understood in that when the adsorbed amount of Co^{2+}–THPP is small, an increase in the number of Co^{2+}–THPP layers enhances the catalytic activity; however, when the adsorbed amount of Co^{2+}–THPP is high enough, a further increase in the number of adsorption layers impedes diffusion of both O_2 and electrolyte towards the inner Co^{2+}–THPP layers, resulting in no additional improvement in the ORR activity and even some extent in a decease that can be seen in the LSV curve of rGO/$(Co^{2+}$–THPP$)_9$ (Figure S8).

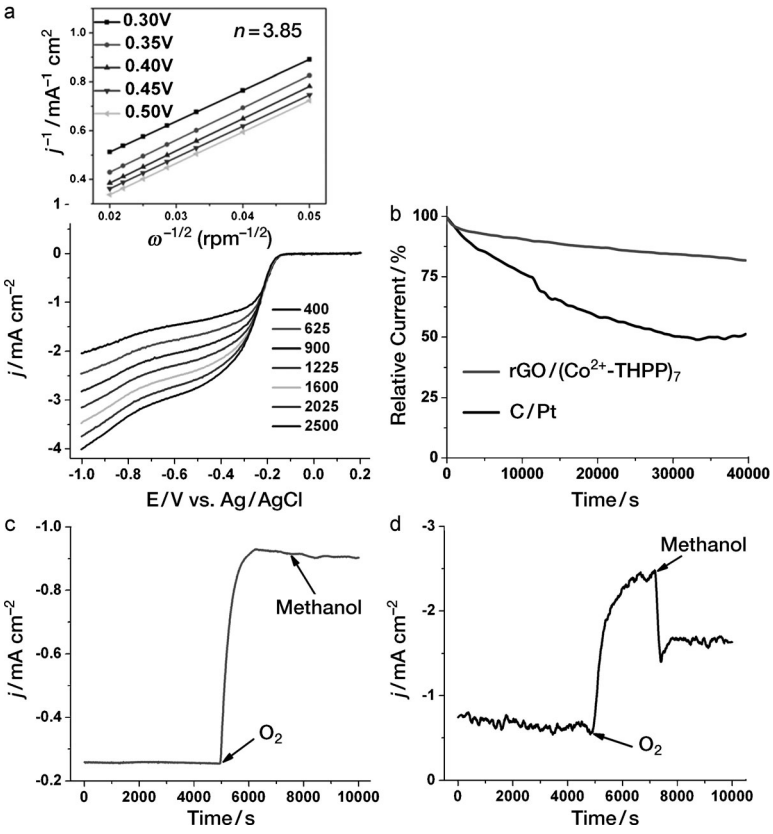

Figure 4. a) LSV on RDE of rGO/$(Co^{2+}$–THPP$)_7$ in O_2-saturated 0.1 M KOH solution with a sweep rate of 10 mV s^{-1} at different rotation rates. Inset: corresponding Koutecky–Levich plots (j^{-1} versus $\omega^{-0.5}$) at different potentials. b) Normalized *I*–*t* chronoamperometric responses of rGO/$(Co^{2+}$–THPP$)_7$ and C/Pt at −0.25 V in O_2-saturated 0.1 M KOH solution at a rotating rate of 1000 rpm. *I*–*t* chronoamperometric responses of c) rGO/$(Co^{2+}$–THPP$)_7$ and d) C/Pt at −0.25 V in 0.1 M KOH solution. The solution is saturated with N_2 from 0 to 5000 s, then by an immediate introduction of O_2. The arrows indicate the point at which 3.0 M methanol is added into the O_2-saturated 0.1 M KOH solution (at 7000 s).

To gain further insight into ORR involving the rGO/$(Co^{2+}$–THPP$)_n$ catalysts, LSV curves on RDE at different rotation rates are recorded (Figure 4a). The electron-transfer number is then calculated to be approximately 3.85 between −0.3 and approximately −0.5 V from the slopes of the Koutecky–Levich plots (the inset in Figure 4a, see details in see details in part S1 in the Supporting Information),[23a] which is consistent with the rotating ring-disk electrode (RRDE) measurements (Figure S9) and similar to the commercial C/Pt (Figure S10), indicating the ORR at the rGO/$(Co^{2+}$–THPP$)_7$ electrodes proceeds by an approximate four-electron reduction pathway.

Except for the activity, the stability is another key parameter for high-performance catalysts.[23b] As seen in Figure 4b, though the current density of both rGO/$(Co^{2+}$–THPP$)_7$ and C/Pt decreases with time, GO/$(Co^{2+}$–THPP$)_7$ has a much slower decay rate. For instance, 80% of the initial catalytic current could be maintained at the rGO/$(Co^{2+}$–THPP$)_7$ electrode after continuous reaction for about 40000 s, whereas only 50% of that is kept for the commercial C/Pt, demonstrating the remarkably stability of rGO/$(Co^{2+}$–THPP$)_7$ in the ORR process.

The catalysts should also be robust in the real application environment.[22a] Specific to the ORR catalysts, the crossover effect must be considered.[23c] As shown in Figure 4c and d, an immediate response in the chronoamperometric curve is observed for C/Pt in O_2-saturated KOH solution with 3.0 M methanol, while no noticeable change for rGO/$(Co^{2+}$–THPP$)_7$ is discerned under the same conditions. The big difference in resistance to methanol is also noted by investigating the CV behaviors of rGO/$(Co^{2+}$–THPP$)_7$ and C/Pt in the O_2-saturated 0.1 M KOH solution containing 3 M methanol (Figure S11). These experimental results unambiguously reveal that rGO/$(Co^{2+}$–THPP$)_7$ has a much better methanol tolerance towards ORR than the commercial C/Pt, namely, a great tolerance to possible crossover effect.

In summary, we have designed and prepares novel C/M-N_x catalysts, rGO/$(Co^{2+}$–THPP$)_n$, for ORR. Compared to other rGO-based materials including rGO/Co^{2+}, rGO/THPP, and rGO/Co_3O_4, rGO/$(Co^{2+}$–THPP$)_n$ exhibits much high electrocatalytic activity. Moreover, in respect to the commercial C/Pt catalysts, rGO/$(Co^{2+}$–THPP$)_n$ shows the comparable electrocatalytic activity, but better stability and increased tolerance to the crossover effect. Such electrocatalytic performances arise from accurate structural control over the rGO/$(Co^{2+}$–THPP$)_n$ composites at the molecular level and corresponding maximization of the synergistic coupling between the Co^{2+}–THPP complexes and the graphene substrate.[24] It can be expected that the LBL approach we employed will open a new avenue for the development of low-cost and high-performance catalysts.

Received: January 27, 2013
Published online: April 15, 2013

Keywords: cobalt · layer-by-layer · multilayers · oxygen reduction reaction · porphyrin

[1] a) M. Winter, R. J. Brodd, *Chem. Rev.* **2004**, *104*, 4245 – 4269; b) A. A. Gewirth, M. S. Thorum, *Inorg. Chem.* **2010**, *49*, 3557 – 3566; c) H. Zhang, P. K. Shen, *Chem. Rev.* **2012**, *112*, 2780 – 2832; d) M. K. Debe, *Nature* **2012**, *486*, 43 – 51.

[2] a) A. Chen, P. Holt-Hindle, *Chem. Rev.* **2010**, *110*, 3767 – 3804; b) Z. Peng, H. Yang, *Nano Today* **2009**, *4*, 143 – 164.

[3] a) Z. Chen, D. Higgins, A. Yu, L. Zhang, J. Zhang, *Energy Environ. Sci.* **2011**, *4*, 3167 – 3192; b) R. Cao, J.-S. Lee, M. Liu, J. Cho, *Adv. Energy Mater.* **2012**, *2*, 816 – 829; c) M.-R. Gao, Y.-F. Xu, J. Jiang, S.-H. Yu, *Chem. Soc. Rev.* **2013**, *42*, 2986 – 3017; d) M.-R. Gao, J. Jiang, S.-H. Yu, *Small* **2012**, *8*, 13 – 27.

[4] a) C. W. B. Bezerra, L. Zhang, K. Lee, H. Liu, A. L. B. Marques, E. P. Marques, H. Wang, J. Zhang, *Electrochim. Acta* **2008**, *53*, 4937 – 4951; b) D. H. Lee, W. J. Lee, W. J. Lee, S. O. Kim, Y.-H. Kim, *Phys. Rev. Lett.* **2011**, *106*, 175502.

[5] a) Y. Zhu, S. Murali, M. D. Stoller, K. J. Ganesh, W. Cai, P. J. Ferreira, A. Pirkle, R. M. Wallace, K. A. Cychosz, M. Thommers, D. Su, E. A. Stach, R. S. Ruoff, *Science* **2011**, *332*, 1537 – 1541; b) Y. Li, W. Zhou, H. Wang, L. Xie, Y. Liang, F. Wei, J.-C. Idrobo, S. J. Pennycook, H. Dai, *Nat. Nanotechnol.* **2012**, *7*, 394 – 400.

[6] R. Jasinski, *Nature* **1964**, *201*, 1212 – 1213.

[7] a) C. T. Carver, B. D. Matson, J. M. Mayer, *J. Am. Chem. Soc.* **2012**, *134*, 5444 – 5447; b) K. M. Kadish, L. Frémond, J. Shen, P. Chen, K. Ohkubo, S. Fukuzumi, M. E. Ojaimi, C. P. Gros, J.-M. Barbe, R. Guilard, *Inorg. Chem.* **2009**, *48*, 2571 – 2582; c) S. Vengatesan, E. Cho, I.-H. Oh, *Korean J. Chem. Eng.* **2012**, *29*, 621 – 626.

[8] X. Li, G. Liu, B. N. Popov, *J. Power Sources* **2010**, *195*, 6373 – 6378.

[9] a) H. Tanaka, T. Yajima, T. Matsumoto, Y. Otsuka, T. Ogawa, *Adv. Mater.* **2006**, *18*, 1411 – 1415; b) J. Malig, C. Romero-Nieto, N. Jux, D. M. Guldi, *Adv. Mater.* **2012**, *24*, 800 – 805; c) M. Shao, X. Xu, J. Han, J. Zhao, W. Shi, X. Kong, M. Wei, D. G. Evans, X. Duan, *Langmuir* **2011**, *27*, 8233 – 8240.

[10] a) Y. Shao, J. Liu, Y. Wang, Y. Lin, *J. Mater. Chem.* **2009**, *19*, 46 – 59; b) N. G. Sahoo, Y. Pan, L. Li, S. H. Chan, *Adv. Mater.* **2012**, *24*, 4203 – 4210; c) S. Wu, Q. He, C. Zhou, X. Qi, X. Huang, Z. Yin, Y. Yang, H. Zhang, *Nanoscale* **2012**, *4*, 2478 – 2483; d) X. Qi, K.-Y. Pu, H. Li, X. Zhou, S. Wu, Q.-L. Fan, B. Liu, F. Boey, W. Huang, H. Zhang, *Angew. Chem.* **2010**, *122*, 9616 – 9619; *Angew. Chem. Int. Ed.* **2010**, *49*, 9426 – 9429.

[11] a) D. Li, R. B. Kaner, *Science* **2008**, *320*, 1170 – 1171; b) D. Li, M. B. Müller, S. Gilje, R. B. Kaner, G. G. Wallace, *Nat. Nanotechnol.* **2008**, *3*, 101 – 105; c) X. Qi, K.-Y. Pu, X. Zhou, H. Li, B. Liu, F. Boey, W. Huang, H. Zhang, *Small* **2010**, *6*, 663 – 669.

[12] a) Y. Xu, Z. Liu, X. Zhang, Y. Wang, J. Tian, Y. Huang, Y. Ma, X. Zhang, Y. Chen, *Adv. Mater.* **2009**, *21*, 1275 – 1279; b) L. Wu, J. Wang, L. Feng, J. Ren, W. Wei, X. Qu, *Adv. Mater.* **2012**, *24*, 2447 – 2452; c) X. Huang, Z. Yin, S. Wu, X. Qi, Q. He, Q. Zhang, Q. Yan, F. Boey, H. Zhang, *Small* **2011**, *7*, 1876 – 1902.

[13] a) X. Huang, X. Qi, F. Boey, H. Zhang, *Chem. Soc. Rev.* **2012**, *41*, 666 – 686; b) X. Huang, Z. Zeng, Z. Fan, J. Liu, H. Zhang, *Adv. Mater.* **2012**, *24*, 5979 – 6004; c) Y. Zheng, Y. Jian, J. Chen, J. Liu, J. Liang, A. Du, W. Zhang, Z. Zhu, S. C. Smith, M. Jaroniec, G. Q. Lu, S. Z. Qiao, *J. Am. Chem. Soc.* **2011**, *133*, 20116 – 20119.

[14] a) Z. Tang, Y. Wang, P. Podsiadlo, N. A. Kotov, *Adv. Mater.* **2006**, *18*, 3203 – 3224; b) L. Li, R. Ma, Y. Ebina, K. Fukuda, K. Takada, T. Sasaki, *J. Am. Chem. Soc.* **2007**, *129*, 8000 – 8007; c) A. Woicik, P. V. Kamat, *ACS Nano* **2010**, *4*, 6697 – 6706.

[15] a) M. Jahan, Q. Bao, K. P. Loh, *J. Am. Chem. Soc.* **2012**, *134*, 6707 – 6713; b) L. Guo, *J. Colloid Interface Sci.* **2008**, *322*, 281 – 286.

[16] Y. Xu, L. Zhao, H. Bai, W. Hong, C. Li, G. Shi, *J. Am. Chem. Soc.* **2009**, *131*, 13490 – 13497.

[17] a) S. Park, J. An, R. D. Piner, I. Jung, D. Yang, A. Velamakanni, S. T. Nguyen, R. S. Ruoff, *Chem. Mater.* **2008**, *20*, 6592 – 6594; b) N. Katsonis, J. Vicario, T. Kudernac, J. Visser, M. M. Pollard, B. L. Feringa, *J. Am. Chem. Soc.* **2006**, *128*, 15537 – 15541.

[18] J. K. Nørskov, J. Rossmeisl, A. Logadottir, L. Lindqvist, J. R. Kitchin, T. Bligaard, H. Jónsson, *J. Phys. Chem. B* **2004**, *108*, 17886 – 17892.

[19] a) D. Conklin, S. Nanayakkara, T.-H. Park, M. F. Lagadec, J. T. Stecher, M. J. Therien, D. A. Bonnell, *Nano Lett.* **2012**, *12*, 2414 – 2419; b) F. Scandola, C. Chiorboli, A. Prodi, E. Lengo, E. Alessio, *Coord. Chem. Rev.* **2006**, *250*, 1471 – 1496.

[20] Z. Li, J. Lu, S. Li, S. Qin, Y. Qin, *Adv. Mater.* **2012**, *24*, 6053 – 6057.

[21] a) Y. Li, J. Xiao, T. E. Shubina, M. Chen, Z. Shi, M. Schmid, H.-P. Steinrück, J. M. Gottfried, N. Lin, *J. Am. Chem. Soc.* **2012**, *134*, 6401 – 6408; b) M. D. Catherine, S. A. Krasnikov, N. N. Sergeeva, A. B. Preobrajenski, N. A. Vinogradov, Y. N. Sergeeva, M. O. Senge, A. A. Cafolla, *Chem. Commun.* **2011**, *47*, 12134 – 12316.

[22] a) H. Yin, H. Tang, D. Wang, Y. Gao, Z. Tang, *ACS Nano* **2012**, *6*, 8288 – 8297; b) Z.-S. Wu, S. Yang, Y. Sun, K. Parvez, X. Feng, K. Müllen, *J. Am. Chem. Soc.* **2012**, *134*, 9082 – 9085.

[23] a) Y. Liang, Y. Li, H. Wang, J. Zhou, J. Wang, T. Regier, H. Dai, *Nat. Mater.* **2011**, *10*, 780 – 786; b) S. Wang, D. Yu, L. Dai, D. W. Chang, J.-B. Baek, *ACS Nano* **2011**, *5*, 6202 – 6209; c) S. Yang, X. Feng, X. Wang, K. Müllen, *Angew. Chem.* **2011**, *123*, 5451 – 5455; *Angew. Chem. Int. Ed.* **2011**, *50*, 5339 – 5343.

[24] a) J. Liang, Y. Zheng, J. Chen, J. Liu, D. Hulicova-Jurcakova, M. Jaroniec, S. Z. Qiao, *Angew. Chem.* **2012**, *124*, 3958 – 3962; *Angew. Chem. Int. Ed.* **2012**, *51*, 3892 – 3896; b) A. M. Chockla, J. T. Harris, V. A. Akhavan, T. D. Bogart, V. C. Holmberg, C. Steinhagen, C. B. Mullins, K. J. Stevenson, B. A. Korgel, *J. Am. Chem. Soc.* **2011**, *133*, 20914 – 20921; c) G. He, Z. Yan, M. Cai, P. K. Shen, M.-R. Gao, H.-B. Yao, S.-H. Yu, *Chem. Eur. J.* **2012**, *18*, 8490 – 8497.

